EXPLORATION OF FARO FREESTYLE 3D LASER SCANNERS AS A METHOD FOR ESTIMATING SURFACE FUEL LOADING FOR WILDLAND FIRE MANAGEMENT

By

JOSEPH RUA

A thesis submitted to the

School of Graduate Studies

Rutgers, The State University of New Jersey

In partial fulfillment of the requirements

For the degree of Master of Science

Graduate Program in Ecology and Evolution

Written under the direction of

JeanMarie Hartman

And approved by

_____

_____

_____

New Brunswick, New Jersey

January, 2018

ABSTRACT OF THE THESIS

Exploration of Faro Freestyle 3D Laser Scanners as A Method for Estimating Surface Fuel Loading for Wildland Fire Management

By JOSEPH RUA

Thesis Director:

Dr. Jean Marie Hartman

To evaluate the effectiveness of the FARO 3D handheld LiDAR unit, I determined when ambient light affected the LiDAR's detection capability. I then used standard destructive harvest methods combined with LiDAR data to examine the relationship between the number of pixels captured by the LiDAR unit with the log transformed dry biomass of the harvest fuels in both leaf-on and leaf-off conditions. Using a Bayesian regression model with a non-informative prior, the analysis showed a weak relationship between pixels and log biomass in leaf-on conditions with an R^2 of 0.22 and a moderately strong relationship between pixels and log biomass in leaf-off conditions with an R^2 of 0.67. The results suggest that handheld LiDAR units have the potential to replace destructive harvest methods under certain conditions, but may not serve as a tool for fire managers to utilize as a regular tool for estimate surface fuel loading.

ACKNOWLEDGEMENTS

I would first like to thank my advisor Dr. Jean Marie Hartman from the Department of Landscape Architecture at Rutgers University. From her sage advice on class choices and research direction to her never-ending patience, there is no doubt in my mind that I would not have been able to survive my graduate program and thesis without her. I could not have hoped for a better advisor, and I am so grateful for her help. I would also like to thank the other members of my committee: Dr. Marci Meixler and Dr. Ed Green. Their input was incredibly valued – especially during my many rounds of edits – and their expertise and experience has strengthened both my thesis and my scientific career.

I would especially like to thank Dr. Michael Gallagher from the United States Forest Service from the Northern Research Forest at Silas Little Experimental Forest who helped me design and develop the scope of work for this thesis as well as allowing me to use the FARO 3D scanner. Dr. Gallagher spent many hours in the field station brainstorming ideas and using his subject matter expertise to help me design this research study. Alongside Dr. Kenneth Clark and Dr. Nicolas Skowronski, this trio of field scientists gave me the inspiration and passion for wildland fire research, and I am forever indebted to all three for their assistance.

Finally, I would like to thank my parents – Michael and Gail; my siblings – Christopher, Michael, and Elizabeth; and my wonderful girlfriend Katherine for all of their support during my times of frustration and constant encouragement that gave me the drive and focus to complete this thesis and this degree.

TABLE OF CONTENTS

TABLE OF FIGURES

TABLE OF TABLES

Chapter 1. Introduction

1.1 Overview

In recent years, wildfires in the United States have been burning with more frequency and more intensity. This trend is only expected to accelerate and intensify with changes in global climate (Abatzoglou 2016, Wotton 2017). While wildfires play important roles in disturbance regimes, they can also threaten both structures and human life – especially in the wildland urban interface (WUI). For ongoing fire spread model development and evaluating treatment effectiveness, estimating forest fuel loading is crucial. Fuel loading, defined as the total weight of dry surface fuel per unit area, is a key factor that regulates fire intensity, as well as rate of spread, during wildfires. Surface fuels are those fuels that are no more than two meters above the ground surface (Keane 2015). Many mathematical models use fuel loading as an input variable (Rothermal 1972 and Andrews 1986, as examples). Therefore, it is vitally important to be able to accurately measure fuel loading. The most accurate method to estimate fuel loading used by researchers involves destructive harvesting and laboratory analysis of fuels, which is time consuming and is not, by definition, “repeatable” (as the plot has been harvested to be dried and measured). One possible way to measure fuel loading more quickly and efficiently is by using remote sensing techniques such as LiDAR (Light Detection and Ranging). With LiDAR, a laser beam is used to scan the forest and collect data representative of the forest’s three dimensional structure. This approach takes considerably less time than destructive sampling, and is repeatable. There are many types of research-grade LiDAR devices available on the market, however, few

consumer-grade devices are available. However, the recently available FARO Freestyle 3D laser scanner is one of few consumer-grade LiDAR devices which is also intended to be more user-friendly. The purpose of this study is to investigate the effectiveness and utility of using a FARO Freestyle 3D LiDAR device to scan surface fuel loads for the development of fuel load estimates, using upland pine-oak forests of the New Jersey Pinelands National Reserve as a test environment. In this study, I report on three tests in order to evaluate the potential for the FARO Freestyle 3D scanner's use in measuring the fuel loading of surface fuels.

The study had three objectives:

1) Determine to what extent outside ambient light affects the accuracy of the FARO Freestyle scanner and explore ways to mitigate this interference.

2) Determine if a relationship exists between biomass and pixel counts when scanning during **leaf-on** time periods.

3) Determine if a relationship exists between biomass and pixel counts when scanning during **leaf-off** time periods

The ultimate objective of the study is to make recommendations as to if and when this tool can be used effectively – both in terms of the time of day as well as the season (leaf-on vs. leaf-off).

1.2 Literature Review

Understanding fire environment characteristics is crucial for predicting fire behavior, estimating risk of catastrophic fire for a given area, and evaluating effectiveness of fuel treatments. The need for this is pressing; according to Barbero et al. (2015), recent modeling predicts that climate change will increase the potential for "Very Large Fires" (defined as the top 5 or 10% of the largest fires) across much of the United States, with the largest increases occurring in the western United States. Some researchers have declared that western forests are burning with uncharacteristic severity and area burned (e.g. Agee 2005) and that the probability of Very Large Wildfires occurring could increase as much as 200 percent through 2060 (Stavros 2014). In order to understand why this is occurring, the most basic tenet of wildland fire research must be examined: the fire triangle.

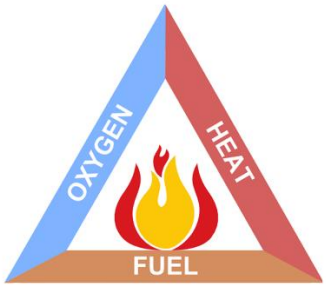

Figure 1.1: The fire triangle[1]

The fire triangle explains the three components that fire needs to exist: oxygen, heat, and fuel. With regard to the latter, fuel structure and total fuel loading in a forest can have a big effect on wildfire intensity and movement (Agee 1996). Since the 1970's, mathematical models have been developed in order to understand and predict the

[1] https://www.firesafetyinfo.co.uk/wp-content/uploads/2013/03/Fire-Triangle.png

movement of fire across landscapes, such as the model developed by Rothermal (1972). Many of these models rely on surface fuel properties as inputs, which are defined by the live and dead forest materials that comprise them. These materials can be in many different shapes, sizes and spatial arrangements such as twigs, leaf and needle litter, branches, and shrubs (Agee 2005). Fuel type and structure effects fire behavior and causes wide variation in the intensity and severity of fire (Despain and Sellers 1977). For instance, fuel load and depth are significant determinants of the likelihood of ignition, the rate of spread, and the intensity of a wildfire (Anderson 1982). Similarly, Mueller et al. (2017) noted that slightly higher values of surface fuel loadings led to a 1.3 times increase in fuel consumption and, thus, a greater peak intensity when compared to a similar experimental plot. Environmental factors can also modulate the role of fuels on fire behavior, and therefore many fire behavior models also include weather and topography (Andrews 1986, Andrews 1999). Therefore, it is fundamentally important to accurately estimate fuel properties to ensure realistic predictions of fire behavior.

Fuels are classified based on their particle type and moisture loss rate, which is inferred from a particle's size classification via timelag categories. Timelag categories relate moisture loss to fuel particle size, based on established standard moisture loss relationships (Keane 2015). More specifically, the timelag categories correspond to the size such that fuel particles with diameters in the ranges of [< 0.25 inches], [0.25 – 1.0 inches], [1.0 – 3.0 inches], and [>3.0] are classified as 1 hour, 10 hour, 100 hour, or 1,000 hour timelag fuels, respectively (Fosberg 1970). These hour categories reflect the rate at which a given dead fuel gains or loses moisture. Fuel moisture plays a significant

role in wildfire spread and intensity (Fryer and Johnson 1988). Different fuel classes and structures also interact with one another and can influence the fireline intensity (in this context, fireline intensity means the same as fire intensity) of a fire (Agee 1996). Horizontal and vertical continuity of fuels also affects the movement of fire across a landscape, as do other related factors such as the fire return interval of a given landscape and time of day. There are different ways of classifying fuel loading as outlined by Hiers (2009), but there is no standard procedure for doing so at areas smaller than stands or fuel beds (Hiers notes that most studies have focused on fire effects and scales of 10 m^2 up to 10,000 ha).

The most accurate method of estimating surface fuel loading is through analysis of destructively harvested surface fuel load material. This method predates remote sensing approaches and continues to serve as the standard for surface fuel load characterization in the research community (Clark 2015; Hudak 2016; Prichard 2014). In this method, all of the surface fuels are harvested down to the duff layer (the layer of fine fuel and leaf litter on top of the soil), sorted by type and fuel timelag category, dried in a drying oven, and weighed for mass. Prior to destructive harvesting, structural aspects of surface fuels, such as shrub height or litter depth, can be recorded as well. While this method is useful, there are certain drawbacks to it. First, it is impossible to repeat an experiment or observation in the same plot over time, since the biomass is harvested. It is also a time consuming process that inherently takes a minimum of two days to complete, considering standard minimum drying times of 48 hours. As result, it is difficult to conduct this method over large spatial scales in a time-efficient manner

and impossible to generate real-time fuel loading estimates during operational burns. Thus, it is important to determine whether technological approaches could mitigate these challenges.

Several remote sensing techniques have been explored for estimating the fuel load mass and arrangement in three dimensional space in forested environments. Spectral scanners (Keane 2001, Saatchi 2007), orthoimagery (Schmidt 2016, Mitsopoulos 2016), and airborne LiDAR units (Skowronski 2007, Garcia 2017), among other less common approaches, have tended to focus on canopy fuel loads in particular. Most of these studies have used sensors that produce data with a medium spatial resolution (see Arroyo 2008 for a list); the drawback is that these reflectance datasets – such as LANDSAT, SPOT, and IKONOS – provide limited information about surface fuel loads (Keane 2001). Studies that have estimated fuel load mass and spatial distribution in forested environments with remote sensing have used LiDAR and have had mixed success. One example is Saatchi et al. (2007), who used an airborne multi-frequency polarimetric synthetic aperture radar (SAR) unit to examine canopy fuel weight, density, and moisture. They found the method resulted in a good agreement with field-based canopy fuel measurements, though there were some limitations concerning areas with large topographical variations. Additionally, using this technique with small forest plot sizes could result in inaccuracies due to errors in geolocation.

LiDAR provides quantitative information about forest structure where other remote sensing approaches don't, lending it to be a more likely approach to estimating fuel loading than reflectance based approaches. Different types of LiDAR devices have

been used to measure structure at different spatial scales, such as satellites (Popescu 2002, Hermosilla 2014), airborne units (Skowronksi 2007), and terrestrial laser scanners (TLS) (Rowell 2016, Chen 2017). Popescu (2002) used satellite LiDAR to look at forests at the landscape level, particularly with respect to mean tree height. Skowronski et al. (2013) used airborne LiDAR to look at stand level structure and estimate total tree biomass and the presence of ladder fuels in combination with forest census data from the Forest Inventory and Analysis program to "characterize forest structure and ladder fuels in the New Jersey Pinelands". Ladder fuels are vegetation, either living or dead, that allow ground fires to travel into the canopy of trees, thereby creating a dangerous crown fire. Eric Rowell (2016) used a TLS in the RxCADRE project to look at fuels at the plot level from a height of 20 meters above the ground and found that fuel height data from the TLS corresponds with field measurements of height.

Surface fuels tend to vary over much smaller spatial scales than canopy fuel characteristics. Hiers et al. (2009) used ground based LIDAR units to measure fuel variation and categorize them into fuel bed cells, noting that wildland fuel cell heights became spatially independent beyond 0.5 m^2 and that fuel cells sow a considerable heterogeneity of fuels at the sub-meter level. Since many LiDAR units have larger resolutions, much of the spatial heterogeneity in the shrub layer is not detected. Keane et al. (2001) states that the high variability of fuels across time and space confounds accurate fuel mapping. Clark (2015) noted how the mass of the shrub layer and the forest floor was related to the time since fire, with biomass increasing as the time after

fire increased. Because this variability occurs at such a fine scale, any review of remote sensing techniques must take this spatial heterogeneity into account.

When evaluating the many methods of remote sensing forest structure, there are several factors that need to be considered. Spatial scale is important, as well as the complexity of the method, the cost of implementation, and the time required for collecting the remotely sensed data. For instance, satellite LiDAR used by Antonarakis et al. (2008) had a resolution of 10 meters, making it ideal to quantify forest structure at large scales and determine differences in cover types such as forest, water, and gravel. However, the high cost and large resolution does not allow for quantifying shrubs and surface fuels – a major source of fuels data in prescribed burns (aside from litter and duff consumed). Terrestrial laser scanners, as used by Rowell et al. (2015), slightly overestimated the height of fuels in small field plots, though it is noted that the long data processing time (six months) means that this TLS approach "is not necessarily an alternative to field measurements of fuels in terms of time savings".

Thus, it is crucial to exploit new technology and instrumentation to improve estimation surface fuel load characteristics, and therefore, new handheld LiDAR devices that are entering the market should be tested as potential fuel measurement tools. By expanding the "tools in the toolbox", fire managers and forest researchers can have more techniques and methods at their disposal to collect data at relevant scales that meet the constraints of field time. The FARO Freestyle is a handheld scanner that has recently entered the market at a price manageable by most fire management agencies, with the stated ability to quickly and easily create high resolution scans of its

environment. SCENE, FARO's image processing and analysis interface, comes with the software at a modest additional charge with the capability of extracting custom information from imagery, making it a strong potential candidate for fuels measurements by researchers and fire managers.

The FARO Scanner Freestyle, produced by FARO Technologies Inc., is a hand operated 3D laser scanner. It captures the structure of objects and environments as it is moved through space using two infrared cameras, one color camera and LED flash unit, and one infrared projector with class 1 laser. The scanner connects to a Microsoft Surface tablet via USB and is intended for use at a distance range of 0.5 meters to 3 meters, though it does have a potential indoor range of up to 10 meters in certain instances. It also has an operating temperature range of 0°C to 40° C (32° F to 104° F) (FARO 2015). The scanner was originally designed for indoor use; however, when used outside, other factors come into play, and, in particular, ambient light can affect the scanner's ability to collect data by making it hard for the scanner to distinguish what is being scanned.

The FARO Freestyle collects data through both a camera on the scanner as well as lasers that collect the points and distance of the target area. When the scanner is collecting information, the scanning screen shows a green "X" for every reference location of material it is receiving a returned laser pulse off of, and a yellow or green shading when it is able to collect a camera feed of the target (yellow for low density, green for sufficient density). The X's are important for tracking purposes, especially during post processing. When the record button is hit, the scanning screen will show

the camera feed of what is being scanned. It does not, however, begin recording the yellow shading and the green X's unless it can distinguish what is being scanned.

Once the scan is complete, a point cloud is generated. A point cloud is the collection of pixels detected by the scanner and their 3D position (along the x, y, and z axes). Post-processing the point cloud data involved the SCENE software provided by FARO. This process optimizes the scan points for 3D viewing and helps to remove duplicate points, or points that were captured from different scanner positions and have similar 3D positions. The process also combined the scanner's high resolution camera images with the point cloud to reducing smearing effects and give more color details. Finally, color balancing helps to reduce the differences in color due to lighting (FARO 2017).

As the use of LiDAR becomes more common in wildland fire research, handheld LiDAR scanners are uniquely positioned to fill an important gap in a researcher's capability – that is, allow the researcher to use LiDAR as a rapid deployment tool to cover large spatial scales over short time frames. This has the potential to change how fuel loading estimations are utilized in fire behavior models and allow fire managers to more accurately quantify the fuel loading of a forest, potentially saving lives and property, while also allowing researchers to better understand how fuel is consumed by fire as it moves across the landscape. Before handheld LiDAR scanners can be utilized in such a manner, however, they must first be tested to determine their fitness for such activities.

1.3 Site Description

Objective One in this study was conducted at the Silas Little Experimental Forest in New Lisbon, New Jersey, USA located within in Brendan T. Byrne State Forest (39.915752, -74.597765). Upland forest vegetation at the Experimental Forest is typical of that observed in other upland forests of Pinelands National Reserve, consisting mostly of a mix of oak (*Quercus*), pitch pine (*Pinus rigida)*, and shortleaf pine (*Pinus echinata)* in the overstory. The oaks are a combination of black oak (*Q. velutina*), white oak (*Q. alba*), chestnut oak (*Q. prinus*), post oak (*Q. stellata*), and blackjack oak (*Q. falcate*). The understory, which is the focus of the study, is dense and consists of oak and pine saplings, scrub oak (*Quercus ilicifolia*), and ericaceous shrubs such as lowbush blueberry (*Vaccinium vacillans*) and black huckleberry (*Gaylussacia baccata*) (McCormick 1998).

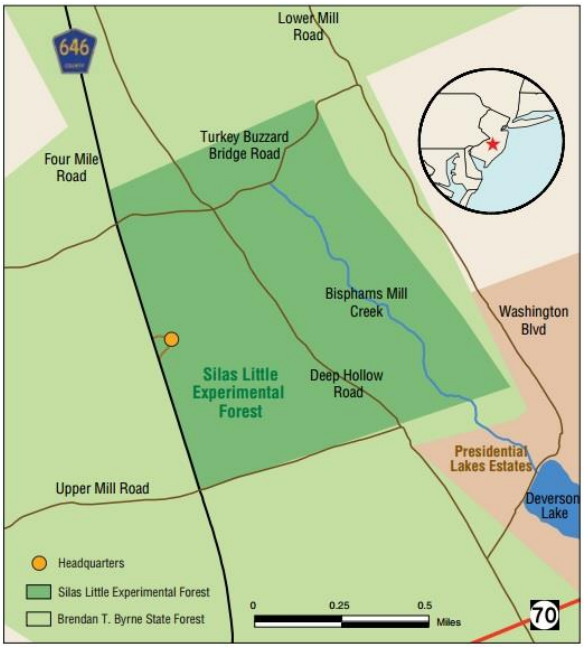

Figure 1.2: Map of Silas Little Experimental Forest[2]

[2] https://www.nrs.fs.fed.us/ef/local-resources/downloads/nrs_inf_19_12-silaslittle-panels.pdf

Work on Objectives Two and Three in this study was conducted in the Greenwood Wildlife Management Area, located approximately 15 miles away from the Silas Little Experimental Forest. These locations were chosen due to their fire history, which is further explained in the methods section. The vegetation composition is nearly identical to the Silas Little Experimental Forest, and the study took place in five separate sites within the management area.

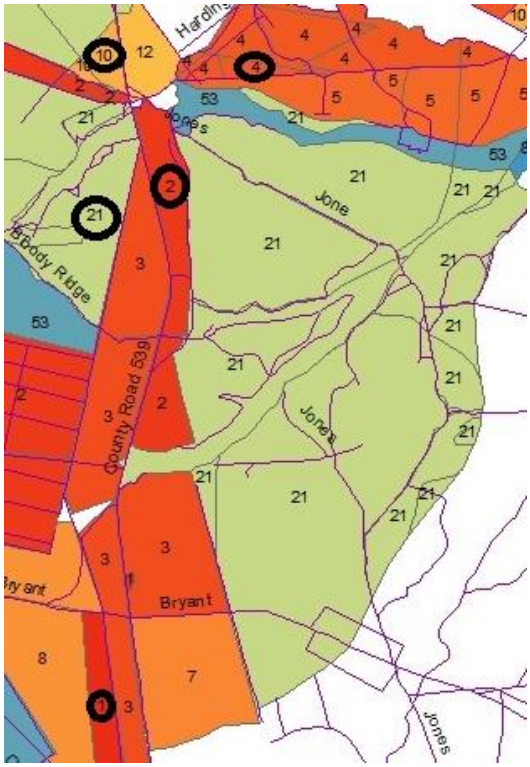

Figure 1.3: Site locations of Objectives Two and Three[3]

In order to get a gradient of cover and biomass levels, we used the fire history of the sites to determine the number of years since the last fire had occurred at the site. This was a useful proxy because the density and complexity of the shrub layer is related to the time since last fire as noted previously in Clark (2015). Using GIS, a layer

[3] Numbers represent years since last fire, and sites used in the study are circled

containing the 50 year fire history of the Pinelands was imported and analyzed. Once the time periods were established, a gradient was chosen of one, two, four, ten, and twenty-one years since the last fire occurred. A map of these sites can be seen in Figure 1.3. The location of these sites can be seen circled in the image below.

Chapter 2. Time Of Day Influence On FARO 3D Scanner's Ability To Estimate Biomass

2.1 Methods

For Objective One, I tested the degree to which ambient light interfered with laser returns and image capture of the FARO Freestyle, which are required for point cloud generation. As such, this test was designed to determine if the scanner was able to effectively record data at selected times of the day when incident ambient light differed.

Scans of vegetation with the FARO Freestyle were conducted under a variety of vegetation and lighting conditions to test the sensor's accuracy under conditions typical in forest census plots. Five study plots were identified as the focal points of this study, by a visual assessment, with the goal of representing a gradient of cover across the five sites. Because the test was not being used to generalize to a study area but rather to explore if the scanner could simply detect scan objects, there was no need to choose the site by stratified random sampling. Scans were conducted in each plot every other hour, from 7:00 AM to 7:00 PM EDT on July 25th, 2016, providing a total of 7 unique ambient lighting conditions. The sunlight was occasionally diffused by passing clouds, meaning that the level of ambient light often varied both within and between plot scans. Sunrise on the test day was 5:50 AM and sunset was 8:16 PM; therefore, all tests were conducted with at least some minor ambient light present.

For each scan, the scanner was mounted on a camera tripod with telescoping legs using a metal pipe and zip ties. This allowed for an overhead scan in which the scanner was parallel to the ground. Each plot in had three poles marking various angle

measurements. These poles were used to ensure that the scanner traversed the same route over all plots in roughly the same time. Poles one and three marked off a 120 degree sector that the scanner would rotate through, and pole two marked off the midpoint of that angle at 60 degrees (Figure 2.1). Each site also had flags placed into the ground to mark off the locations that the tripod legs would be placed each time, to ensure scans were repeated over the same locations.

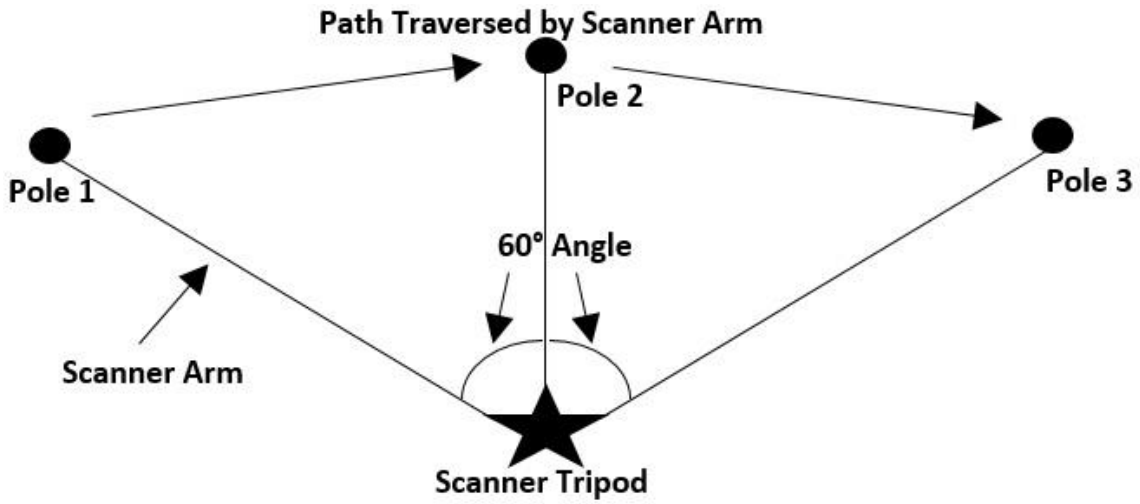

Figure 2.1: Overhead diagram of Objective One plot

For each of the plots, the scanner was tested in four different ways. Preliminary usage suggested that the scanner would likely be more effective when moving slowly than capturing data from a static location. As such, there were four different conditions: a 1 meter high stationary scan, a 1 meter high moving scan, a 1.5 meter high stationary scan, and a 1.5 meter high moving scan. Figure 2.2 illustrates the site set-up. For all of the stationary scans, the scanner was lined up to pole 2. For all moving scans, the scanner was positioned at pole 1 and, upon the start of recording, would slowly transverse the 120 degree sector and end at pole 3. There were a total of 140

combinations of time, plot and condition (5 plots x 4 conditions at each x 7 timeslots). Each of these timeslots took roughly an hour to complete.

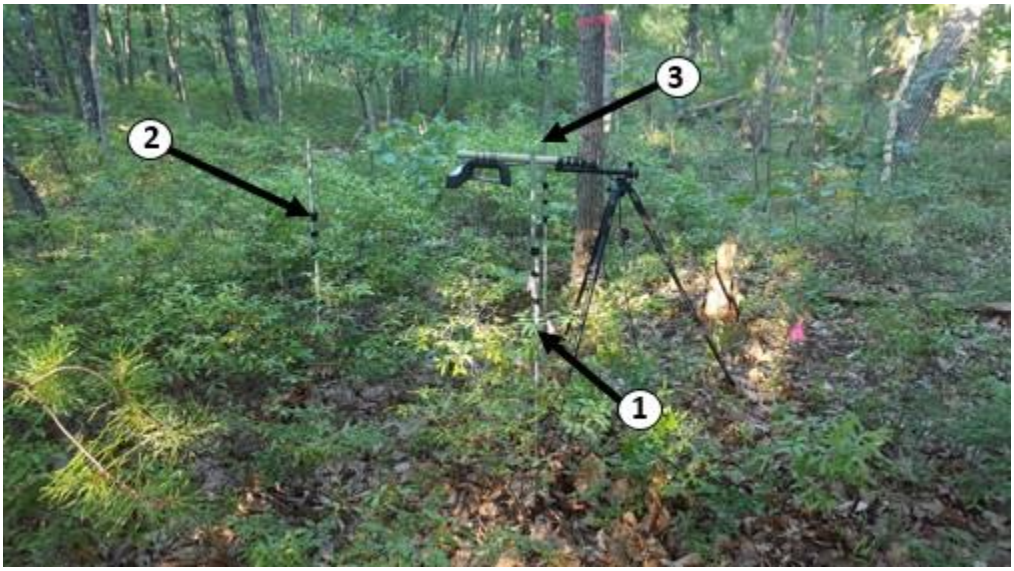

Figure 2.2: Site design, Objective One

The same process was used for all scanning. The record button would be hit on the tablet, and the researcher would wait for the scanner to begin detecting features as previously described. If the scanner began to detect features, the scan continued for 60 seconds (crossing pole 2 and the 30 second mark), then stopped, and the tripod was moved into position 2. If, after 15 seconds, the scanner did not pick up any features, the scan was stopped and restarted. This was repeated 3 times for a total of 4 attempts. After either the first successful attempt or the fourth unsuccessful attempt, the scanner was moved into the correct position for the next condition and the process was repeated. For the moving scans, the scanner traversed the scanning area for a total of 60 seconds in a single pass. After all 4 positions were completed, the scanner was moved to the next plot. The only data recorded aside from the point clouds of the successful scans was whether or not the scanner was able to detect features at each

position for that timeslot. This data is a binary pass/fail value. If the scanner was able to detect features at any point during the four attempts at that condition (thereby creating a point cloud), it was marked as a "success." If the scanner failed to detect any scanning features during the four attempts at that condition, it was marked as a "fail." The quality or pixel counts of the point clouds were not relevant in this Objective – only the ability of the scanner to record point cloud data at all.

2.2 Results

For Objective One, the results of the test can be seen in Table 2.1. The specific results for each plot and scan attempt can be seen in Appendix A.

Table 2.1: Percent Success Rate of Objective One Scans Performed at Different Timeslots

Time of Day	1 Meter stationary		1 Meter Moving		1.5 Meter Stationary		1.5 Meter Moving		Total	
	N	%	N	%	N	%	N	%	N	%
7:00 AM	5	100%	4	80%	5	100%	5	100%	19	95%
9:00 AM	3	60%	4	80%	4	80%	5	100%	16	80%
11:00 AM	1	20%	0	0%	0	0%	0	0%	1	2%
1:00 PM	2	40%	2	40%	1	20%	2	40%	7	35%
3:00 PM	1	20%	1	20%	1	20%	1	20%	4	20%
5:00 PM	2	40%	3	60%	3	60%	2	40%	10	50%
7:00 PM	4	80%	5	100%	5	100%	5	100%	19	95%
Total	18	51%	19	54%	19	54%	20	57%	76	54%

The overall rate of success for each time period can be seen in Table 2.1. As the table makes clear, the most successful times for scanning were 7:00 AM and 7:00 PM EST, with the 9:00 AM timeslot a close second. Both the 7:00 AM and 7:00 PM timeslots had a success rate of 95%, with 19 of the 20 scans conducted at that time being successful. The other times of the day were less successful, and often the only times that the scans were successful at 11:00 AM, 1:00 PM, and 3:00 PM was when a cloud

bank rolled in and diffused some of the ambient light. Out of the 140 total scans (20 scans per timeslot multiplied by 7 timeslots), 54% of the scans were able to detect features when the scan was active (76/140).

2.3 Discussion

It is clear from Table 2.1 that ambient sunlight at sufficient levels will interfere with the sensor's ability to capture data. The most successful scan times were those that had very low to intermediate direct sunlight overhead. The results of the test were consistent with what we expected, and thus helped to inform the methods utilized in Objectives Two and Three. It is unclear how the test would have been affected if the day had been overcast as opposed to partly sunny. The few times that the scanner did collect data points around midday were when clouds did cover the direct sunlight, causing the light to be more diffuse. Even then, not all of the scans that were performed when those clouds were present collected data. This suggests that some other factor, such as the shading effect of the forest canopy, worked in conjunction with the cloud to absorb or reflect enough light for the scanner to detect data.

Chapter 3. Understory Biomass Measurements During Leaf-On And Leaf-Off Period

3.1 Methods

In these Objectives, the scanner was tested on both leaf-on and leaf-off shrubs at five different sites in the Greenwood Wildlife Management Area. Within each of the different sites, six individual plots were chosen to represent a range of cover and structure density within each of the fire histories. As such, it was unnecessary to choose the site by stratified random sampling since the scanner was simply being calibrated and tested.

Once the plots were chosen and flagged, a 1 meter by 1 meter PVC square was placed around the flag. Once the square was placed, a six to twelve inch buffer zone was cleared on all sides of the PVC square. This removed all of the biomass that was leaning into the scan area. This was necessary in order to make sure that the biomass that was harvested in the plot square was the only biomass scanned by the Freestyle scanner. Otherwise, extra biomass could have been detected by the scanner and recorded as pixels but not harvested and weighed for the biomass reading. Generally, any biomass rooted in the square was kept for harvesting. The rare exceptions occurred where the branches of a shrub extended too far past the study square or above the scanner and into locations the scanner could not pick up. This setup can be seen in Figure 3.1 below. The tripod used in Objective 1 was only 1.5 meters high and, in order to ensure the scanner was 2 meters above the plots, had its' legs extended using metal piping and duct tape. Two meters became the choice height for scanning because it allowed for the

whole square to be completely scanned, and also accounted for very tall shrubs in some of the plots.

Figure 3.1: Scan plot design for Objectives Two and Three

Using the lessons learned in Objective One, each plot was measured using a moving scan at a height of 2 meters (as surface fuels are defined as biomass <2m above the ground; Keane 2012) that lasted a total of 120 seconds (there were diminishing returns on detection past this point). These scans took place between 7:00AM and 8:00 AM because, as seen in Objective One, the low levels of ambient light allowed for the most accurate collection of data. Once the scan was completed, the plot square was moved to the next plot and that plot was scanned as described above. Due to time constraints related to the ambient light levels in the forest, only one site could be scanned per day. The scan setup for Objective Two can be seen in Figure 3.2 below. Upon completion of all six scans, the plots were then destructively harvested. All of the surface fuels were harvested down to the duff layer and bagged and labeled. These materials were then dried in a convection oven for at least 48 hours at 70°C. Once the drying was completed, the biomass of each site was weighed and recorded.

Figure 3.2: Site design for Objectives Two and Three

All harvests occurred on the same day as scanning except for one site (Site 2; two years since last fire) due to weather. These scans took place between September and October 2016 as noted in Table 3.1.

Table 3.1: Time and Date of Objective Two Scans

Site	Date of Scan	Time of Scan	Date of Harvest	Years Since Last Fire
1	9/14/2016	7:00 AM	9/14/2016	1
2	9/19/2016	7:00 AM	9/21/2016	2
3	10/5/2016	7:00 AM	10/5/2016	4
4	10/17/2016	7:00 AM	10/17/2016	10
5	9/23/2016	7:00 AM	9/23/2016	21

Objective Three data collection was similar to that of Objective Two, with the key difference being the leaf-off conditions. The same five sites were chosen based on the fire history in the Greenwood Management Area (i.e. one, two, four, ten and twenty-one years since last fire). These six plots were prepared identically to the six leaf-on plots in each site. All scans and harvests occurred on the same day as scanning except for one site (Site 2; two years since last fire). Ambient light interference did not allow for

plots 5 and 6 in Site 2 to be scanned the same day as the other four plots. Those scans were completed two days later, and all six sites were then harvested on that day. The table of scan dates for Objective Three can be seen below in Table 3.2.

Table 3.2: Time and Date of Objective Three Scans				
Site	Date of Scan	Time of Scan	Date of Harvest	Years Since Last Fire
1	12/14/2016	8:00 AM	12/14/2016	1
2	12/19/2016	7:30 AM	12/21/2016	2
3	12/23/2016	7:30 AM	12/23/2016	4
4	12/22/2016	7:30 AM	12/22/2016	10
5	12/21/2016	7:30 AM	12/21/2016	21

3.2 Raw Data Post Processing

Each scan resulted in an unprocessed point cloud of pixels from the scan. These scans included the pixels of the shrubs and ground cover in the plot squares as well as a fair portion of the shrubs and ground cover outside the square. The first step in post processing the data was to refine the point clouds using the FARO SCENE software's automatic post-processing feature. To refine the point clouds, SCENE combined the laser scan data with the imagery captured by the onboard camera to create a fuller and more accurate scan image. This post process task took approximately 15 minutes per scan. An example of a point cloud can be seen in Figure 3.3.

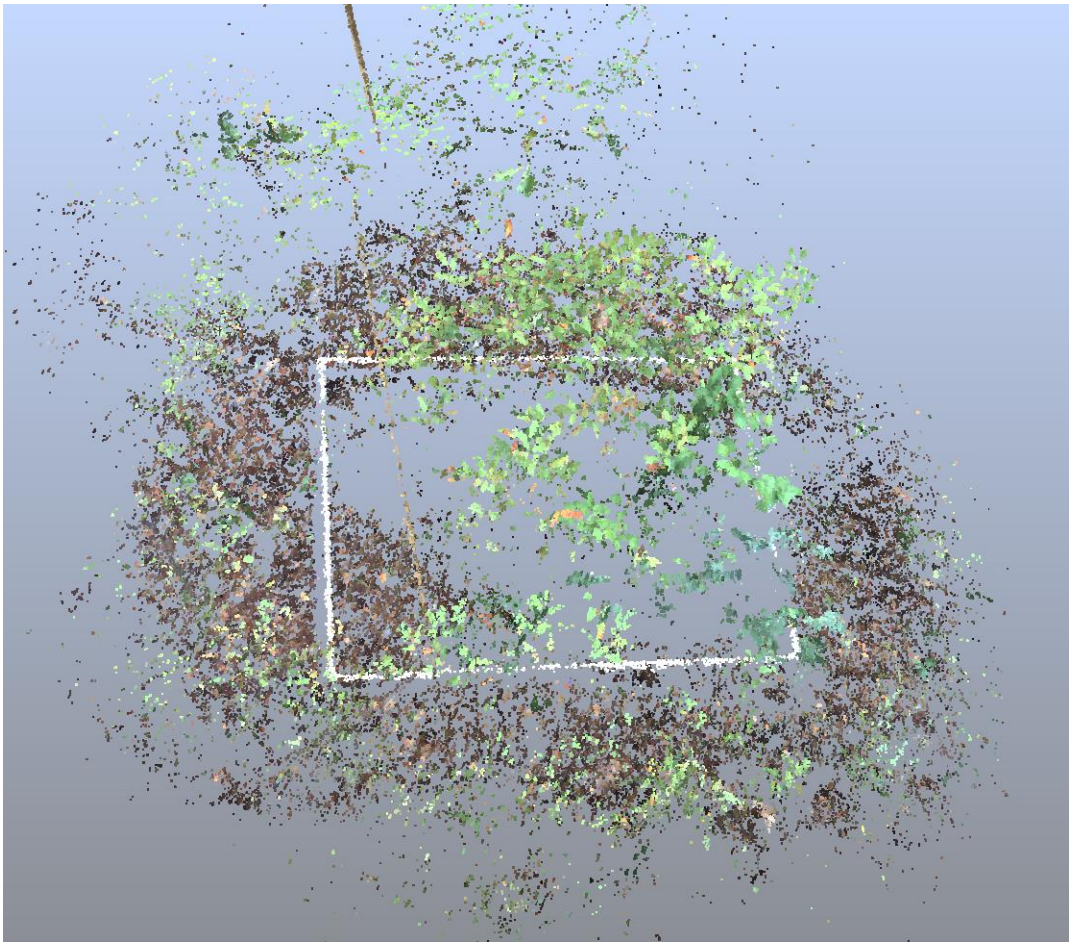

Figure 3.3: Point cloud from a scan during Objective Two

Once the refined point cloud was created, the next step was to eliminate all of the excess pixels in the image outside of the square by using a “clipping box” to remove any excess pixels. This required orienting the scan correctly along the X, Y, and Z axes. Once the scan was aligned, the clipping box was then similarly oriented along the X, Y, and Z axes. Using the white PVC square as the boundary, the clipping boxes were moved along the X and Y axes and aligned with the inside of the PVC pipe square. Once those were in line, the Z axis was raised or lowered to both align with the top of the PVC square as well as the top of the shrubs that were scanned. This “clipping box” eliminated all of the excess pixels outside of the site as well as any stray pixels captured

above the shrub layer. Once the pixels were clipped, the data files were exported from Scene and then imported into CloudCompare, an open source 3D point cloud and mesh processing software, to perform the pixel counts.

3.3 Data Analysis

Data was analyzed using the OpenBUGS software, version 3 (Lunn 2009). The biomass data were log transformed using Microsoft Excel. A simple Bayesian regression was used to determine if a relationship existed between pixel counts and the log biomass, and an r-squared value was used to determine the strength of the relationship by examining the 95% credible interval of beta:

$$y_i = \alpha + \beta x_i + e_i, \quad i = 1, 2, \dots, n$$

Where:

$e_i \sim N(0, \sigma^2); \quad \alpha \sim N(0, 1.0 \times 10^6); \quad \beta \sim N(0, 1.0 \times 10^6); \quad \sigma \sim UNIF(0,400)$

Non-informative priors were utilized in the model. The model was run using a 2000 iteration “burn in” to achieve convergence and then run for an additional 20,000 iterations. Appendix B contains the OpenBUGS syntax used to run the regression equation above for determining whether a relationship exists between log biomass and pixel counts.

The second step in the analysis was to ensure that the results were demonstrable over all five categories of time since last fire – one, two, four, ten, and twenty one years. For this, the slope and intercept data from the two, four, ten, and twenty one year categories were compared to the one year to determine if any differences existed between them. The equation and priors used can be seen below.

$$mu_i = \beta 1 + \beta 2x1_i + \beta 3x2_i + \beta 4x3_i + \beta 5x4_i + \beta 6z_i +$$

$$\beta 7x1_i z_i + \beta 8x2_i z_i + \beta 9x3_i z_i + \beta 10x4_i z_i \quad i = 1,2, \dots, n$$

Where:

$\beta 1 \sim N(0, 1.0 \times 10^6)$; $\beta 2 \sim N(0, 1.0 \times 10^6)$; $\beta 3 \sim N(0, 1.0 \times 10^6)$; $\beta 4 \sim N(0, 1.0 \times 10^6)$; $\beta 5 \sim N(0, 1.0 \times 10^6)$; $\beta 6 \sim N(0, 1.0 \times 10^6)$; $\beta 7 \sim N(0, 1.0 \times 10^6)$; $\beta 8 \sim N(0, 1.0 \times 10^6)$; $\beta 9 \sim N(0, 1.0 \times 10^6)$; $\beta 10 \sim N(0, 1.0 \times 10^6)$; $\tau \sim \gamma(0.001, 0.001)$

Non-informative priors were utilized in the model. The model was run using a 2000 iteration "burn in" to achieve convergence and then run for an additional 20,000. Appendix C contains the OpenBUGS syntax used to run the slope and intercept comparison.

3.4 Results

Objective Two

The results of the biomass measurements and pixel counts for Objective Two are listed in Table 3.3. Figure 3.4 illustrates a scatter plot of the log biomass vs. pixel count data.

Table 3.3: Biomass (g) and Pixel Counts for Objective Two Plots

		Plot One	Plot Two	Plot Three	Plot Four	Plot Five	Plot Six	Average Biomass	St. Dev.	St. Error
Site One	Biomass	111.85	80.94	271.44	169.08	156.8	35.04	137.53	82.05	33.5
	Pixels	247,631	287,606	215,801	231,926	70,945	146,614	200,087	78,381	31,998.79
Site Two	Biomass	366.59	297.75	362.23	245.15	208.12	238.14	286.33	67.03	27.37
	Pixels	1,102,368	861,591	808,656	887,457	572,919	670,241	802,205	158,108	64,547.47
Site Three	Biomass	450.36	417.05	957.24	306.73	234.93	275.71	440.38	266.45	108.78
	Pixels	1,499,290	1,036,666	634,204	528,076	375,596	463,940	756,295	430,823	175,882.80
Site Four	Biomass	291.25	395.12	607.52	634.72	414.57	467.63	468.47	131.66	53.75
	Pixels	354,012	576,047	315,539	93,694	139,132	847,667	387,682	283,412	115,702.48
Site Five	Biomass	369.26	626.17	597.98	455.14	256.89	456.08	460.59	138.11	56.38
	Pixels	644,080	917,624	552,781	451,483	408,653	376,065	558,448	201,750	82,364.22

For the regression, the 95% credible interval of beta must not include 0 if a relationship exists. The 2.5 percent and 97.5 percent values for Objective Two are 0.00015 and 0.0066, respectively, with the mean value being 0.0033. In this credible interval, 0 is not included as a possible value. This indicates that **there is a relationship** between the biomass and the pixel counts for Objective Two because both the 2.5 percent and 97.5 percent values are above zero. The coefficient values appear low because of the nature of the data.

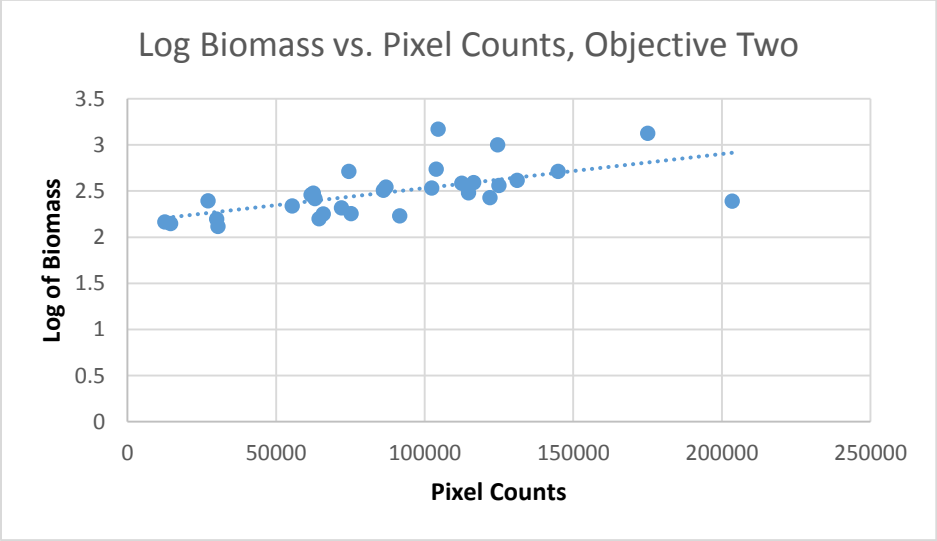

Figure 3.4: A plot of the log biomass vs. pixel counts for Objective Two

To determine the strength of that relationship, an R-Squared value was calculated and the 95% credible interval examined. The 2.5 percent and 97.5 percent values of R-Squared are 0.14 and 0.62, respectively, with the mean value being 0.22. The low R-Squared mean value indicates **that there is a weak relationship** between the biomass and the pixel counts.

A comparison of slope and intercept data was calculated and the 95% credible interval examined. The 2.5 percent and 97.5 percent values are illustrated in Table 3.4

Table 3.4 Objective Three Credible Intervals of Slope and Intercept Differences

		Mean Value	2.5%	97.5%
One Year	Slope	2.01	1.473	2.641
	Intercept	0.0002366	-0.002841	0.002785
Two Years	Slope	0.02721	-1.089	1.111
	Intercept	0.0002738	-0.002497	0.003449
Four Years	Slope	0.4503	-0.25200	1.125
	Intercept	-0.00006429	-0.002618	0.003029
Ten Years	Slope	0.6875	-0.007109	1.314
	Intercept	-0.0003435	-0.003022	0.002767
Twenty One Years	Slope	0.4086	-0.4405	1.154
	Intercept	0.0001673	-0.002468	0.003458

If any of the credible intervals for two, four, ten or twenty one years does not include zero as a potential value, it means that there is evidence that the relationship varies by fire history. As seen in Table 3.4, every credible interval contain zero as a possible value. Thus, the relationship does not vary by time since last fire.

Objective Three

The results of the biomass measurements and pixel counts for Objective Three are listed in Table 3.5. Figure 3.5 illustrates a scatter plot of the log biomass vs. pixel count data.

Table 3.5: Biomass (g) and Pixel Counts for Objective Three Plots

		Plot One	Plot Two	Plot Three	Plot Four	Plot Five	Plot Six	Average Biomass	St. Dev.	St. Error
Site One	Biomass	130.54	170.69	179.18	179.95	245.14	390.76	216.04	93.17	178.01
	Pixels	30,430	91,630	65,858	72,223	203,454	116,486	97,180	59,357	72,947.66
Site Two	Biomass	363.88	247.63	146.2	140.06	207.24	158.62	210.61	85.68	175.63
	Pixels	125,066	27,083	12,564	14,542	71,994	64,438	52,605	43,500	34,845.65
Site Three	Biomass	261.84	322.39	385.71	288.37	300.84	348.43	317.93	44.4	299.8
	Pixels	63,069	86,070	112,467	61,789	62,466	87,009	78,812	20,285	70,530.47
Site Four	Biomass	218.62	302.62	269.09	413.36	517.02	342.02	343.79	107.51	299.9
	Pixels	55,424	114,754	121,984	131,058	144,912	102,388	111,753	31,134	99,043.05
Site Five	Biomass	547.96	516.04	1003.31	1482.39	157.71	1340.09	841.25	518.69	629.05
	Pixels	103,874	74,490	124,540	104,486	30,006	175,082	102,080	48,577	82,248.19

For the regression, the 95% credible interval of beta must not include 0 if a relationship exists. The 2.5 percent and 97.5 percent values for Objective Two are 0.019 and 0.055,

respectively, with the mean value being 0.037. In this credible interval, 0 is not included as a possible value. This indicates that **there is a relationship** between the biomass and the pixel counts for Objective Three because both the 2.5 percent and 97.5 percent values are above zero. The coefficient values appear low because of the nature of the data.

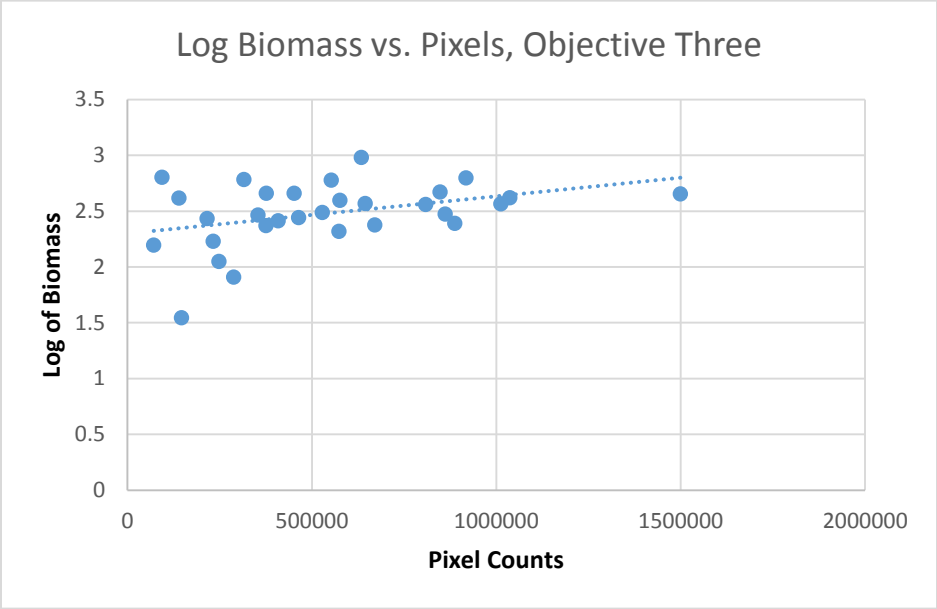

Figure 3.5: A plot of the log biomass vs. pixel counts for Objective Three

To determine the strength of that relationship, an R-Squared value was calculated and the 95% credible interval examined. The 2.5 percent and 97.5 percent values of R-Squared are 0.62 and 0.82, respectively, with the mean value being 0.67. This indicates **that there is a moderately strong relationship** between the biomass and the pixel counts.

A comparison of slope and intercept data was calculated and the 95% credible interval examined. The 2.5 percent and 97.5 percent values are illustrated in Table 3.6.

Table 3.6 Objective Three Credible Intervals of Slope and Intercept Differences

		Mean Value	2.50%	97.50%
One Year	Slope	0.001776	-0.0002025	0.003925
	Intercept	2.132	1.887	2.352
Two Year	Slope	0.001082	-0.002497	0.004503
	Intercept	0.01462	-0.2751	0.3189
Four Year	Slope	0.001009	-0.005753	0.007217
	Intercept	0.1464	-0.3789	0.7228
Ten Year	Slope	0.001713	-0.002964	0.00587
	Intercept	-0.002578	-0.4825	0.5229
Twenty One Year	Slope	0.004616	0.001309	0.007903
	Intercept	0.03955	-0.3241	0.4093

If any of the credible intervals for two, four, ten or twenty one years does not include zero as a potential value, it means that there is evidence that the relationship varies by fire history. As seen in Table 3.6, the credible interval for the slope of the twenty one years since last fire category does not contain zero as a possible value. Thus, the relationship does vary by fire history, or time since last fire.

3.5 Discussion

Given the results of the exploration, there is a demonstrated, albeit weak, relationship between the biomass and the pixel counts in Objective Two and a moderately strong relationship in Objective Three. This means that the biomass can be estimated more accurately with leaves off the plant as compared to the leaves on the plant. There were potential issues with the laser penetrating the brush to capture hidden features, or that certain branches were hid by the shadows of the plant.

The r-squared value was much higher for the leaf off scans when compared to the leaf on scans (mean of 0.22 vs mean of 0.67, respectively). One potential explanation is that the surface area of the leaves blocked some of the smaller branches and twigs from being detected by the scanner during leaf on, potentially

underestimating the biomass that that branch provides. Additionally, there may be some discrepancy given the surface area to biomass ratio of the leaves, since leaves provided a lot of pixels comparably given their biomass contribution. This, in turn, could make the scans more inaccurate in terms of their pixel to log biomass relationship.

Additionally, there is no evidence to suggest that leaf-on scans would vary given the fire history of the sire (time since last fire). This is not the case with leaf-off scans, however, as the analysis has indicated that the relationship between pixels and log biomass could be influenced by time since last fire as a covariate. Given the small number of plots per site (six), it would be prudent to repeat the test with more sites per plot to see if the analysis yields similar results.

Chapter 4. Conclusions

The aim of this study was to determine if the FARO Freestyle would be a useful tool for fire managers to quickly evaluate shrub fuel loading over large areas. The results of this study demonstrate that the FARO Freestyle has potential for use in individual projects with the objective of estimating shrub mass without destructive sampling. The results demonstrated that the scanner is more accurate when no leaves are present on the plant, making the FARO Freestyle a potential seasonal tool. Remote sensing is still an important way forward for fire managers as it allows them to be able to cover much larger geographic areas in shorter time spans. The FARO Freestyle's utility as a daily tool for fire managers is unlikely, however, given the limitations due to ambient light interference. There is no doubt in the researcher's mind that the FARO Freestyle definitely fits into that future; other scanners, however, still need to be tested in order to determine which is best for the job. More specifically, it may be more useful to use remote sensing techniques such as the helicopter borne LiDAR unit used in Skowronski et al. (2007) as it allows for a large coverage area. Obvious drawbacks exist, such as the potential cost of using such a technique as well as issues surrounding the scale of study. There exists some potential to couple the use of helicopter or satellite borne technologies in conjunction with handheld scanners to record fine-grain data.

There are several different avenues forward for future research. First, this study only developed the relationship between the biomass and pixel counts of a pine-oak forest. It would be interesting to see if different forest types yield different results. For example, would forests whose shrubs have, on average, much broader leaves still be

good candidates for the Freestyle scanner used as it was in this study? Additionally, further research may also be directed at evaluating the predictive power of the relationship. While this relationship was determined using real data collected, it would be interesting to conduct more scans in the Pine Barrens to increase the predictive power and accuracy of the relationship. These scans could then be post processed and their pixel counts could be plugged into the relationship developed here. The predicted biomass levels could then be compared to the actual biomass weights that were harvested to see how accurate the model is at predicting the biomass at the sites. This would demonstrate that the relationship has some predictive power, thereby eliminating the need for destructive harvests altogether when using the scanner. Additionally, the scanner could be utilized in a multidirectional scan as opposed to a top down only scan. This could help capture features hidden by leaves and twigs at certain angles and give a more robust scan to analyze.

In a similar vein, the scanner may also prove useful in evaluating the shrub layer post fire. By scanning a shrub layer before and after a fire, such as a controlled burn, the scanner may be able to give accurate estimates on fuel consumption. This has implications both for understanding the intensity of a fire as well as evaluating the level of risk mitigation that was accomplished through the treatment. By understanding fuel consumption after a fire, researchers may be able to better understand the resiliency of different forest types to fire as a disturbance regime. Given the 3D scans, there is also potential to look at not just the total biomass of the shrub layer consumed but also the structure of the layer as well. It is well documented that the structure of fuels in a forest

shrub layer has a large effect on the fire's intensity and rate of spread (Agee 1996, 2005). By looking at the structure of the understory, researchers may be able to gain valuable insight into how a fire moves through a landscape on a smaller scale. This movement may then be scaled up to understand fire on larger scales. This area of research may be the strongest use of the FARO Freestyle going forward.

Literature Cited

Abatzoglou, J. T., & Williams, A. P. (2016). Impact of anthropogenic climate change on wildfire across western US forests. *Proceedings of the National Academy of Sciences of the United States of America, 113*(42), 11770-11775. doi:10.1073/pnas.1607171113

Agee, J. K. (1996). The influence of forest structure on fire behavior. *Proceedings of the 17th Annual Forest Vegetation Management Conference,* 52-68.

Agee, J. K., & Skinner, C. N. (2005). Basic principles of forest fuel reduction treatments. *Forest Ecology and Management, 211*(1), 83-96.

Anderson, H. E. (1982). *Aids to determining fuel models for estimating fire behavior.* (No. General Technical Report INT-122).USDA Forest Service, Intermountain Forest and Range Experiment Station.

Andrews, P. L. (1986). *BEHAVE: Fire behavior prediction and fuel modeling system-BURN subsystem, part 1.* (No. General Technical Report INT-194).USDA Forest Service, Intermountain Forest and Range Experiment Station.

Andrews, P. L., & Bevins, C. D. (1999). BEHAVE fire modeling system: Redesign and expansion. *Fire Management Notes, 59*(2), 16-19.

Antonarakis, A. S., Richards, K. S., & Brasington, J. (2008). Object-based land cover classification using airborne LiDAR. *Remote Sensing of Environment, 112*(6), 2988-2998. doi:10.1016/j.rse.2008.02.004

Arroyo, L. A., Pascual, C., & Manzanera, J. A. (2008). Fire models and methods to map fuel types: The role of remote sensing. *Forest Ecology and Management, 256*(6), 1239-1252.

Barbero, R., Abatzoglou, J. T., Kolden, C. A., Larkin, N. K., & Stocks, B. (2015). Climate change presents increased potential for very large fires in the contiguous united states. *International Journal of Wildland Fire, 24*(7), 892-899. doi:10.1071/WF15083

Bessie, W., & Johnson, E. (1995). The relative importance of fuels and weather on fire behavior in subalpine forests. *Ecology, 76*(3), 747-762.

Chen, Y., Zhu, X., Yebra, M., Harris, S., & Tapper, N. (2017). Development of a predictive model for estimating forest surface fuel load in australian eucalypt forests with LiDAR data. *Environmental Modelling and Software, 97*, 61-71. doi:10.1016/j.envsoft.2017.07.007

Chuvieco, E., Cocero, D., Riano, D., Martin, P., Martınez-Vega, J., de la Riva, J., & Perez, F. (2004). Combining NDVI and surface temperature for the estimation of live fuel moisture content in forest fire danger rating. *Remote Sensing of Environment, 92*(3), 322-331.

Clark, K. L., Skowronski, N., Hom, J., Duveneck, M., Pan, Y., Van Tuyl, S., Cole,J., Patterson,M., Maurer, S. (2009). Decision support tools to improve the effectiveness of hazardous fuel reduction treatments in the new jersey pine barrens. *International Journal of Wildland Fire, 18*(3), 268-277.

Clark, K. L., Skowronski, N., & Gallagher, M. (2015). Fire management and carbon sequestration in pine barren forests. *Journal of Sustainable Forestry, 34*(1), 125-146. doi:10.1080/10549811.2014.973607

Clark, K. L., Skowronski, N., Gallagher, M., Renninger, H., & Schäfer, K. (2012). Effects of invasive insects and fire on forest energy exchange and evapotranspiration in the new jersey pinelands. *Agricultural and Forest Meteorology, 166-167*, 50-61. doi:10.1016/j.agrformet.2012.07.007

Clark, K. L., Skowronski, N., Gallagher, M., Carlo, N., Farrell, M., & Maghirang, M. R. (2010). *Assessment of canopy fuel loading across a heterogeneous landscape using LiDAR.* (No. JFSP Project Number: 10-1-02-14).

Despain, D. G., & Sellers, R. E. (1977). Natural fire in yellowstone national park. *Western Wildlands, 4*, 20-24.

FARO Technologies. (2015). *FARO scanner Freestyle3D user manual.* (User Manual).FARO Technologies Inc.

Flannigan, M. D., & VanWagner, C. E. (1991). Climate change and wildfire in canada. *Canadian Journal of Forest Research, 21*(1), 66-72.

Fosberg, M. A., Lancaster, J. W., & Schroeder, M. J. (March 1970). Fuel moisture response--drying relationships under standard and field conditions. *Forest Science, 16*(1), 121-128.

Fryer, G., & Johnson, E. (1988). Reconstructing fire behaviour and effects in a subalpine forest. *Journal of Applied Ecology, 25*(3), 1063-1072.

Garcia, M., Saatchi, S., Balzter, H., Casas, A., Koltunov, A., Ustin, S., . . . Garcia-Gutierrez, J. (2017). Quantifying biomass consumption and carbon release from the california rim fire by integrating airborne LiDAR and landsat OLI data. *Journal of Geophysical Research: Biogeosciences, 122*(2), 340-353. doi:10.1002/2015JG003315

Hermosilla, T., Coops, N., Ruiz, L., Moskal, L. M., & Kazakova, A. N. (2014). Estimation of forest structure and canopy fuel parameters from small-footprint full-waveform LiDAR data. *International Journal of Wildland Fire, 23*(2), 224-233.

Hiers, J. K., O'Brien, J. J., Mitchell, R., Grego, J. M., & Loudermilk, E. L. (2009). The wildland fuel cell concept: An approach to characterize fine-scale variation in fuels and fire in frequently burned longleaf pine forests. *International Journal of Wildland Fire, 18*(3), 315-325.

Hudak, A. T., Bright, B. C., Dickinson, M. B., Kremens, R. L., Loudermilk, E. L., O'Brien, J. J., Hornsby, B.S., Ottmar, R. D. (2016). Measurements relating fire radiative energy density and surface fuel consumption - RxCADRE 2011 and 2012. *International Journal of Wildland Fire, 25*(1), 25-37. doi:10.1071/WF14159

Keane, R. E. (2013). Describing wildland surface fuel loading for fire management: A review of approaches, methods and systems. *International Journal of Wildland Fire, 22*(1), 51-62.

Keane, R. E. (2015). ***Wildland fuel fundamentals and applications***. Switzerland: Springer International Publishing.

Keane, R. E., Burgan, R., & van Wagtendonk, J. (2001). Mapping wildland fuels for fire management across multiple scales: Integrating remote sensing, GIS, and biophysical modeling. *International Journal of Wildland Fire, 10*(4), 301-319.

Lunn, D., Spiegelhalter, D., Thomas, A. and Best, N. (2009), The BUGS project: Evolution, critique and future directions. Statistics in Medicine, 28: 3049–3067. doi:10.1002/sim.3680

McCormick, J. (1998). The vegetation of the new jersey pine barrens. In R. T. Forman (Ed.), *Pine barrens: Ecosystem and landscape* (pp. 229-241) Rutgers University Press.

Mitsopoulos, I., Mallinis, G., Karali, A., Giannakopoulos, C., & Arianoutsou, M. (2016). Mapping fire behaviour under changing climate in a mediterranean landscape in greece. *Regional Environmental Change, 16*(7), 1929-1940. doi:10.1007/s10113-015-0884-0

Mueller, E. V., Skowronski, N., Clark, K., Gallagher, M., Kremens, R., Thomas, J. C., . . . Simeoni, A. (2017). Utilization of remote sensing techniques for the quantification of fire behavior in two pine stands. *Fire Safety Journal, 91*, 845-854. doi:10.1016/j.firesaf.2017.03.076

Popescu, S. C., Wynne, R. H., & Nelson, R. F. (2002). Estimating plot-level tree heights with lidar: Local filtering with a canopy-height based variable window size. *Computers and Electronics in Agriculture, 37*(1), 71-95. doi:10.1016/S0168-1699(02)00121-7

Prichard, S. J., Karau, E. C., Ottmar, R. D., Kennedy, M. C., Cronan, J. B., Wright, C. S., & Keane, R. E. (2014). Evaluation of the CONSUME and FOFEM fuel consumption models in pine and mixed hardwood forests of the eastern united states. *Canadian Journal of Forest Research, 44*(7), 784-795. doi:10.1139/cjfr-2013-0499

Rothermel, R. C. (1972). *A mathematical model for predicting fire spread in wildland fuels.* (No. Research Paper INT-115).USDA Forest Service, Intermountain Forest and Range Experiment Station.

Rowell, E. M., Seielstad, C. A., & Ottmar, R. D. (2016). Development and validation of fuel height models for terrestrial lidar - RxCADRE 2012. *International Journal of Wildland Fire, 25*(1), 38-47. doi:10.1071/WF14170

Saatchi, S., Halligan, K., Despain, D. G., & Crabtree, R. L. (2007). Estimation of forest fuel load from radar remote sensing. *IEEE Transactions on Geoscience and Remote Sensing, 45*(6), 1726-1740.

Schmidt, I. T., O'Leary, J. F., Stow, D. A., Uyeda, K. A., & Riggan, P. J. (2016). Use of ultra-high spatial resolution aerial imagery in the estimation of chaparral wildfire fuel loads. *Environmental Monitoring and Assessment, 188*(12) doi:10.1007/s10661-016-5656-x

Skowronski, N. S., Clark, K. L., Gallagher, M., Birdsey, R. A., & Hom, J. L. (2014). Airborne laser scanner-assisted estimation of aboveground biomass change in a temperate oak–pine forest. *Remote Sensing of Environment, 151*, 166-174.

Skowronski, N. S., Haag, S., Trimble, J., Clark, K. L., Gallagher, M. R., & Lathrop, R. G. (2015). Structure-level fuel load assessment in the wildland-urban interface: A fusion of airborne laser scanning and spectral remote-sensing methodologies. *International Journal of Wildland Fire, 25*(5), 547-557.

Skowronski, N., Clark, K., Nelson, R., Hom, J., & Patterson, M. (2007). Remotely sensed measurements of forest structure and fuel loads in the pinelands of new jersey. *Remote Sensing of Environment, 108*(2), 123-129.

Stavros, E. N., Abatzoglou, J. T., McKenzie, D., & Larkin, N. K. (2014). Regional projections of the likelihood of very large wildland fires under a changing climate in the contiguous western united states. *Climatic Change, 126*(3-4), 455-468. doi:10.1007/s10584-014-1229-6

Stratton, R. D. (2004). Assessing the effectiveness of landscape fuel treatments on fire growth and behavior. *Journal of Forestry, 102*(7), 32-40.

Thaxton, J. M., & Platt, W. J. (2006). Small-scale fuel variation alters fire intensity and shrub abundance in a pine savanna. *Ecology, 87*(5), 1331-1337.

Wotton, B.,M., Flannigan, M.,D., & Marshall, G. A. (2017). Potential climate change impacts on fire intensity and key wildfire suppression thresholds in canada. *Environmental Research Letters, 12*(9)

Appendix A: Success of Individual Objective One Plots

An “x” indicates a successful detection of scan features, while an “0” indicates that no scan features were detected. Each scan was attempted four times before moving to the next plot and/or scan type.

	Start Time	7:00am	9:00am	11:00am	1:00pm	3:00pm	5:00pm	7:00pm
Site 1	**1 Meter Moving**	**X**	**0**	**X**	**0**	**0**	**0**	**X**
	1 Meter Stationary	**X**	**0**	**0**	**0**	**0**	**X**	**X**
	1.5 Meter Moving	**X**	**0**	**0**	**0**	**0**	**X**	**X**
	1.5 Meter Stationary	**X**	**X**	**0**	**0**	**X**	**0**	**X**
Site 2	**1 Meter Moving**	**X**	**X**	**0**	**X**	**X**	**0**	**X**
	1 Meter Stationary	**X**	**X**	**0**	**X**	**X**	**0**	**X**
	1.5 Meter Moving	**X**	**X**	**0**	**0**	**X**	**0**	**X**
	1.5 Meter Stationary	**X**	**X**	**0**	**0**	**0**	**0**	**X**
Site 3	**1 Meter Moving**	**X**	**0**	**0**	**0**	**0**	**0**	**0**
	1 Meter Stationary	**X**	**X**	**0**	**0**	**0**	**0**	**X**
	1.5 Meter Moving	**X**	**X**	**0**	**0**	**0**	**0**	**X**
	1.5 Meter Stationary	**X**	**X**	**0**	**X**	**0**	**0**	**X**
Site 4	**1 Meter Moving**	**X**	**X**	**0**	**0**	**0**	**X**	**X**
	1 Meter Stationary	**X**	**X**	**0**	**X**	**0**	**X**	**X**
	1.5 Meter Moving	**X**	**X**	**0**	**X**	**0**	**X**	**X**
	1.5 Meter Stationary	**X**	**X**	**0**	**0**	**0**	**X**	**X**
Site 5	**1 Meter Moving**	**X**	**X**	**0**	**X**	**0**	**X**	**X**
	1 Meter Stationary	**0**	**X**	**0**	**0**	**0**	**X**	**X**
	1.5 Meter Moving	**X**	**X**	**0**	**0**	**0**	**X**	**X**
	1.5 Meter Stationary	**X**	**X**	**0**	**X**	**0**	**X**	**X**
	End Time	7:47am	9:47am	11:46am	1:46pm	3:47pm	5:47pm	7:46pm

Appendix B: OpenBUGS Syntax for Analysis of Log Biomass and Pixel Count Relationship

Objective Two

Model

```
{
        for (i in 1:N)
                {
                mu.bio[i] <- alpha + beta*(y[i] /10000)
                logbio[i] ~ dnorm(mu.bio[i],tau)
                        }
                        alpha ~ dnorm(0.0,0.000001)
                        beta ~ dnorm(0.0,0.000001)
                        sigma ~ dunif(0,400)
                        tau <- 1/(sigma*sigma)
        for (i in 1:N)
                {
                residual[i] <- logbio[i] - mu.bio[i]
                num[i] <- (residual[i])*(residual[i])
                }
RSS <- sum(num[])
rsq <- (RSS/CTSS)
}
```

Data

```
list(y = c(247631, 287606, 215801, 231926, 70945, 146614, 1012368, 861591, 808656,
887457, 572919, 670241, 1499290, 1036666, 634204, 528076, 375596, 463940, 354012,
576047, 315539, 93694, 139132, 847667, 644080, 917624, 552781, 451483, 408653,
376065),

logbio = c(2.048635988, 1.9081632, 2.433673847, 2.228092239, 2.195346058,
1.544564097, 2.564180614, 2.47385177, 2.558984416, 2.389431898, 2.318313817,
2.376832349, 2.653820101,2.620188126, 2.981020838, 2.486756255, 2.370938479,
2.440452518, 2.464265934, 2.596729013, 2.78356058, 2.802582183, 2.617597872,
2.669902365, 2.567332265, 2.796692257, 2.776686659, 2.658145005, 2.413115276,
2.659041028),
        CTSS = 2.436774,
#       lb_bar=2.47996,
        N = 30 )
```

Inits

```
list(alpha=1,beta=1, sigma=1)
```

Objective Three

Model

```
{
        for (i in 1:N)
                {
                mu.bio[i] <- alpha + beta*(y[i] /10000)
                logbio[i] ~ dnorm(mu.bio[i],tau)
                        }
                        alpha ~ dnorm(0.0,0.000001)
                        beta ~ dnorm(0.0,0.000001)
                        sigma ~ dunif(0,400)
                        tau <- 1/(sigma*sigma)
        for (i in 1:N)
                {
                residual[i] <- logbio[i] - mu.bio[i]
                num[i] <- (residual[i])*(residual[i])
                }
RSS <- sum(num[])
rsq <- (RSS/CTSS)
}
```

Data

```
list(y = c(30430, 91630, 65858, 75223, 203454, 116486, 125006, 27083, 12564, 14542,
71994, 64438, 63069, 86070, 112467, 61789, 62466, 87009, 55424, 114754, 121984,
131058, 144912, 102388, 103874, 74490, 124540, 04486, 30006, 175082),

logbio = c(2.115743608, 2.232208078, 2.253289532, 2.255151851, 2.389414182,
2.591910101, 2.560958186, 2.393803258, 2.164947373, 2.146314122, 2.316473584,
2.200357946, 2.418035992, 2.508381562, 2.586260899, 2.459950077, 2.47833558,
2.542115541, 2.33968989, 2.480897627, 2.429897559, 2.616328449, 2.713507343,
2.534051503, 2.738748857, 2.712683367, 3.001435141, 3.170962477, 2.197859232,
3.127133966),
        CTSS = 2.130974,
#       lb_bar=2.489228,
        N = 30 )
```

Inits

```
list(alpha=1,beta=1, sigma=1)
```

Appendix C: OpenBUGS Syntax for Slope and Intercept Comparison

Objective Two

Model

```
{
        for (i in 1:N)
                {
                y[i] ~ dnorm(mu[i], tau)
                mu[i] <- b1 + b2*x1[i] + b3*x2[i] + b4*x3[i] + b5*x4[i] + b6*z[i] +
                        b7*x1[i]*z[i] + b8*x2[i]*z[i] + b9*x3[i]*z[i] + b10*x4[i]*z[i]
                }
        b1 ~ dnorm(0.0,0.000001)
        b2 ~ dnorm(0.0,0.000001)
        b3 ~ dnorm(0.0,0.000001)
        b4 ~ dnorm(0.0,0.000001)
        b5 ~ dnorm(0.0,0.000001)
        b6 ~ dnorm(0.0,0.000001)
        b7 ~ dnorm(0.0,0.000001)
        b8 ~ dnorm(0.0,0.000001)
        b9 ~ dnorm(0.0,0.000001)
        b10 ~ dnorm(0.0,0.000001)
        tau ~ dgamma(0.001,0.001)
}
```

Data

```
        list(x1 = c(0,0,0,0,0,0,1,1,1,1,1,1,0,0,0,0,0,0,0,0,0,0,0,0,0,0,0,0,0,0),
            x2 = (0,0,0,0,0,0,0,0,0,0,0,0,1,1,1,1,1,1,0,0,0,0,0,0,0,0,0,0,0,0),
            x3 = (0,0,0,0,0,0,0,0,0,0,0,0,0,0,0,0,0,0,1,1,1,1,1,1,0,0,0,0,0,0),
            x4 = (0,0,0,0,0,0,0,0,0,0,0,0,0,0,0,0,0,0,0,0,0,0,0,0,1,1,1,1,1,1),
            z = c(247.631, 287.606, 215.801, 231.926, 70.945, 146.614,
                1012.368, 861.591, 808.656, 887.457, 572.919, 670.241, 1499.290,
                1036.666, 634.204, 528.076, 375.596, 463.940, 354.012, 576.047,
                315.539, 93.694, 139.132, 847.667, 644.080, 917.624, 552.781, 451.483,
                408.653, 376.065),
            y = c(2.048635988, 1.9081632, 2.433673847, 2.228092239, 2.195346058,
                1.544564097, 2.564180614, 2.47385177, 2.558984416, 2.389431898,
                2.318313817, 2.376832349, 2.653820101,2.620188126, 2.981020838,
                2.486756255, 2.370938479, 2.440452518, 2.464265934, 2.596729013,
                2.78356058, 2.802582183, 2.617597872, 2.669902365, 2.567332265,
                2.796692257, 2.776686659, 2.658145005, 2.413115276, 2.659041028),
        N = 30)
```

Inits

```
        list(b1=1, b2=1, b3=1, b4=1, b5=1, b6=1, b7=1, b8=1, b9=1, b10=1,tau=1)
```

Objective Three

Model

```
{
        for (i in 1:N)
                {
                y[i] ~ dnorm(mu[i], tau)
                mu[i] <- b1 + b2*x1[i] + b3*x2[i] + b4*x3[i] + b5*x4[i] + b6*z[i] +
                        b7*x1[i]*z[i] + b8*x2[i]*z[i] + b9*x3[i]*z[i] + b10*x4[i]*z[i]
                }
        b1 ~ dnorm(0.0,0.000001)
        b2 ~ dnorm(0.0,0.000001)
        b3 ~ dnorm(0.0,0.000001)
        b4 ~ dnorm(0.0,0.000001)
        b5 ~ dnorm(0.0,0.000001)
        b6 ~ dnorm(0.0,0.000001)
        b7 ~ dnorm(0.0,0.000001)
        b8 ~ dnorm(0.0,0.000001)
        b9 ~ dnorm(0.0,0.000001)
        b10 ~ dnorm(0.0,0.000001)
        tau ~ dgamma(0.001,0.001)
}
```

Data

```
        list(x1 = c(0,0,0,0,0,0,1,1,1,1,1,1,0,0,0,0,0,0,0,0,0,0,0,0,0,0,0,0,0,0),
            x2 = (0,0,0,0,0,0,0,0,0,0,0,0,1,1,1,1,1,1,0,0,0,0,0,0,0,0,0,0,0,0),
            x3 = (0,0,0,0,0,0,0,0,0,0,0,0,0,0,0,0,0,0,1,1,1,1,1,1,0,0,0,0,0,0),
            x4 = (0,0,0,0,0,0,0,0,0,0,0,0,0,0,0,0,0,0,0,0,0,0,0,0,1,1,1,1,1,1),
            z = c(30.430, 91.630, 65.858, 75.223, 203.454, 116.486, 125.006, 27.083,
            12.564,
                14.542, 71.994, 64.438, 63.069, 86.070, 112.467, 61.789, 62.466, 87.009,
                55.424, 114.754, 121.984, 131.058, 144.912, 102.388, 103.874, 74.490,
                124.540, 104.486, 30.006, 175.082),
            y = c(2.115743608, 2.232208078, 2.253289532, 2.255151851, 2.389414182,
                2.591910101, 2.560958186, 2.393803258, 2.164947373, 2.146314122,
                2.316473584, 2.200357946, 2.418035992, 2.508381562, 2.586260899,
                2.459950077, 2.47833558, 2.542115541, 2.33968989, 2.480897627,
                2.429897559, 2.616328449, 2.713507343, 2.534051503,  2.738748857,
                2.712683367, 3.001435141, 3.170962477, 2.197859232, 3.127133966),
        N = 30)
```

Inits

```
        list(b1=1, b2=1, b3=1, b4=1, b5=1, b6=1, b7=1, b8=1, b9=1, b10=1,tau=1)
```